Supporting Information

Park et al. 10.1073/pnas.1304238110
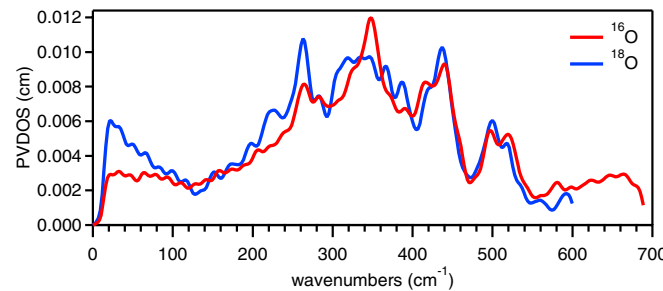
Fig. S1. NRVS spectra of the Fe(IV)$_2$ complexes of **1** with ^{16}O (red) and ^{18}O (blue) isotopes.
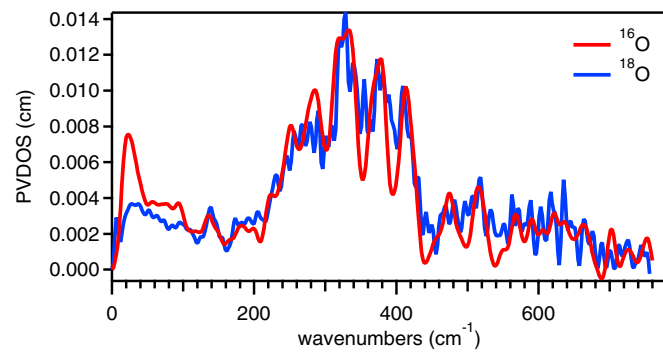
Fig. S2. NRVS spectra of the Fe(IV)$_2$ complexes of **2** with ^{16}O (red) and ^{18}O (blue) isotopes.
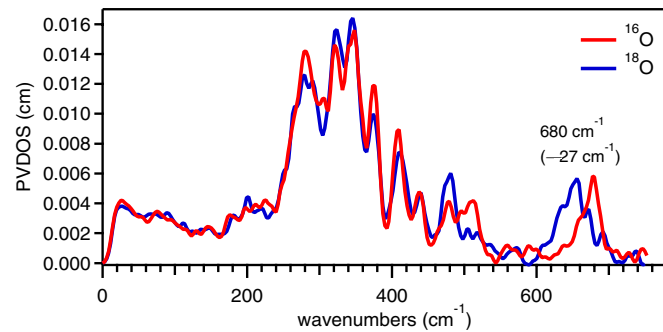
Fig. S3. NRVS spectra of the Fe(III)Fe(IV) complexes of **2** with ^{16}O (red) and ^{18}O (blue) isotopes.
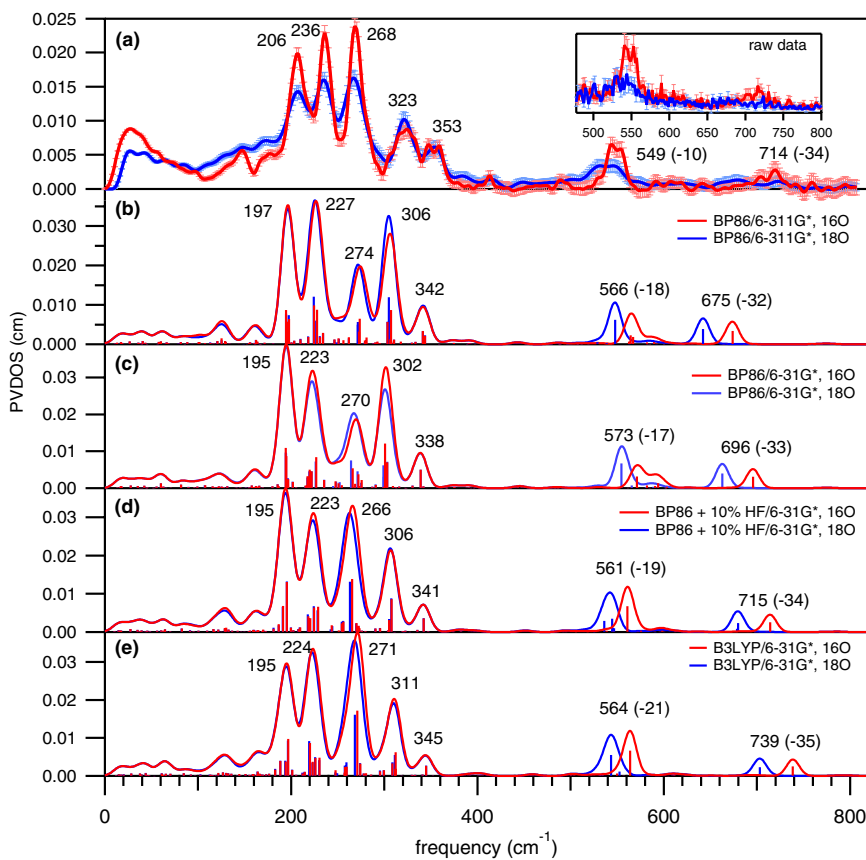
Fig. S4. PVDOS of the Fe(III)$_2$ precursor of **1** obtained by (A) experiment and DFT calculations using (B) pure BP functional and 6–311G* basis set, (C) pure BP functional and 6–31G* basis set, (D) 10% HF/90% BP functional and 6–31G* basis set, and (D) 20% HF/90% BP functional (i.e., B3LYP) and 6–31G* basis set. Frequencies are denoted with $^{16/18}$O isotopic shifts in parentheses. Compared with the data in (A), the simulation in (B) shows over- and underestimated energies for the symmetric and anti-symmetric Fe-μO stretch, respectively, and the intensity of the peak at 274 cm^{-1} is underestimated. The simulation in (C) shows that using the double-zeta basis set reproduces the simulation in (B) although stretch (>500 cm^{-1}) and bend (<400 cm^{-1}) modes are up- and down-shifted, respectively, compared with (B). Addition of 10% HF exchange (C vs. D) improves the energies of the Fe-μO stretches and the intensity of the peak at 266 cm^{-1}, although using 20% HF exchange in (E) overestimates the energy of the antisymmetric Fe-μO stretch.
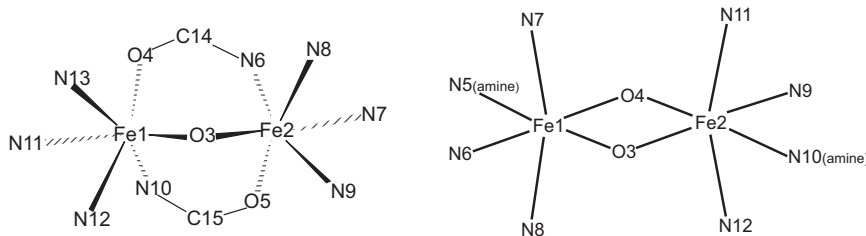

Fig. S5. Core structures of **1** (*Left*) and **2** (*Right*) and their atomic numbering schemes.
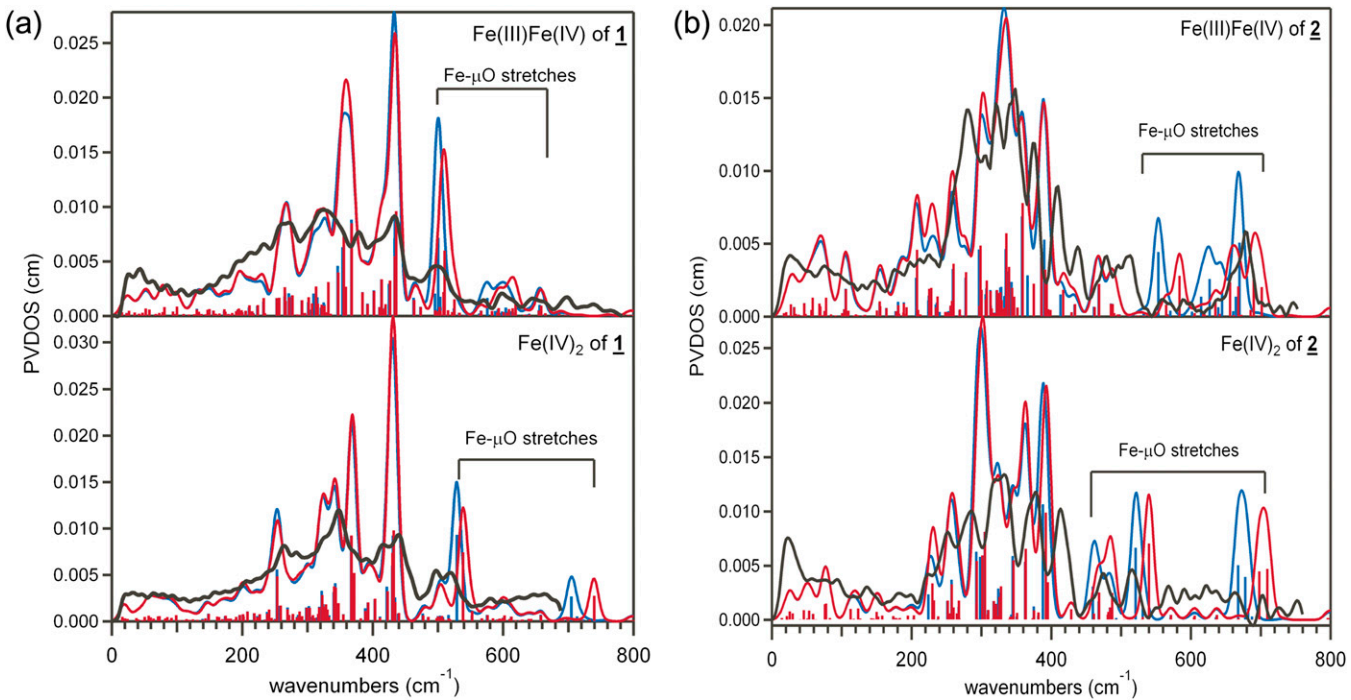
Fig. S6. DFT-predicted NRVS spectra (red, ^{16}O; blue, ^{18}O) of the Fe(III)Fe(IV) (*Upper*) and Fe(IV)$_2$ (*Lower*) complexes of (*A*) **1** and (*B*) **2**. Experimental data are presented in black. DFT well reproduces the three-peak pattern of **1** and its insensitivity to ^{18}O isotope labeling. Note that the DFT calculations of **1** predict a 10 cm^{-1} isotopic shift for the Fe-µO symmetric stretch [at 539 cm^{-1} for the Fe(IV)$_2$ complex]. This shift was not experimentally observed (Fig. S1), due to the low resolution (~8 cm^{-1}) of NRVS and the elevated noise level of the high-energy region. The DFT calculations of **2** reproduce the five peaks in the energy region below 450 cm^{-1}, although their energies are underestimated by ~20 cm^{-1}. Their insensitivity to ^{18}O isotope labeling is also reproduced in the DFT calculations, and the isotopic shifts for the Fe-µO stretch modes of the Fe(IV)$_2$ complex of **2** were obscured (Fig. S2) due to the high noise level of the data.
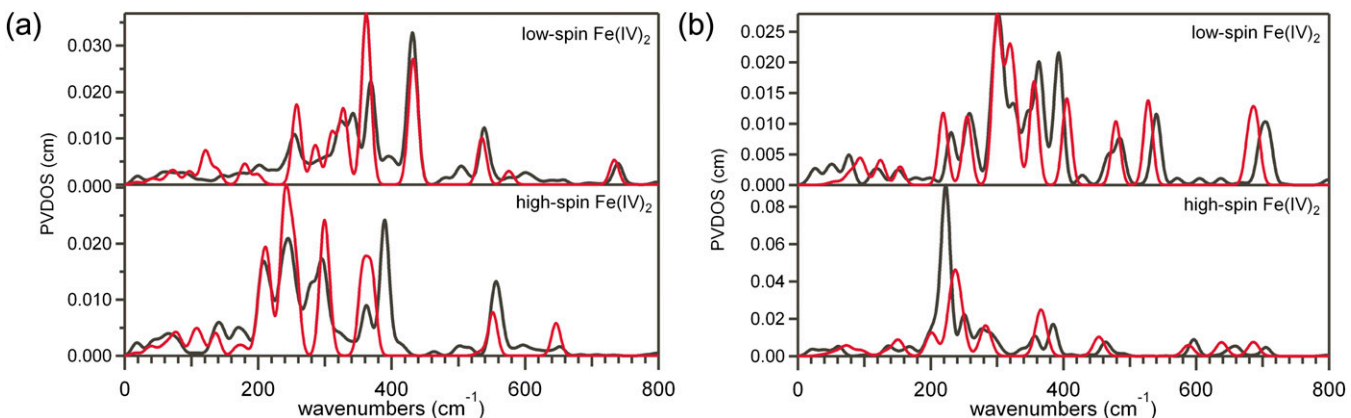
Fig. S7. DFT (black) and normal coordinate analysis (NCA; red) predicted NRVS spectra of the low-spin (*Upper*) and high-spin (*Lower*) Fe(IV)$_2$ complexes of (*A*) **1** and (*B*) **2**. Due to the large size of the Hessian matrices in redundant internal coordinates and sizable off-diagonal elements obtained from DFT calculations, NCA analyses were performed using a more limited number of atoms. The core structures of DFT-optimized geometries shown in Fig. S5 were used to fit DFT-predicted NRVS spectra, with the diagonal elements of the Hessian matrices used as initial guesses for the force constants. Internal coordinate force constants thus obtained are given in Tables S5 and S6.
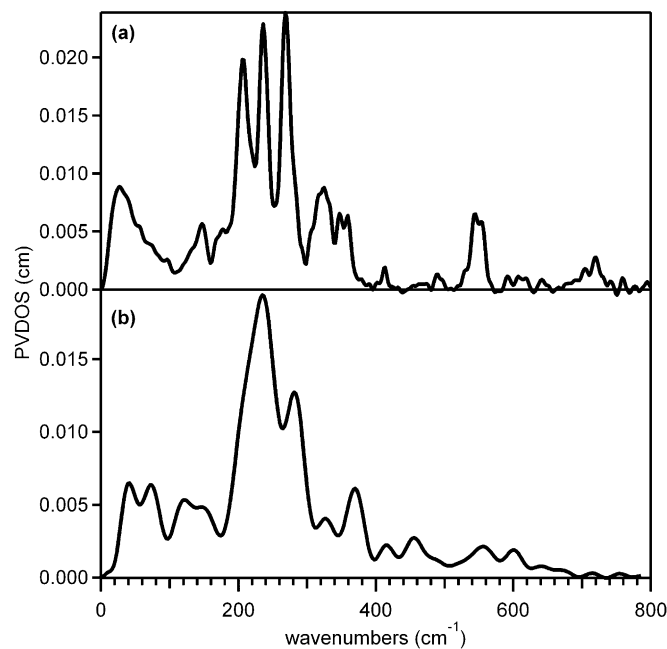
Fig. S8. Experimental NRVS spectra of high-spin Fe(III)$_2$ complexes with (*A*) a mono-oxo bridge (reproduced from Fig. 2*C*) and (*B*) a di-hydroxo bridge ([Fe$_2$(μ-OH)$_2$(6Me$_2$-BPP)$_2$]$^{2+}$, reproduced from ref. 1. Considering that variation in the Fe oxidation state causes only minor changes in NRVS spectra and using the di-hydroxo structure to model a di-oxo core, the data on these high-spin Fe(III)$_2$ complexes experimentally support the DFT predictions for the high-spin Fe(IV)$_2$ analogs of **1** and **2** (Fig. 7). Spectrum (*A*) shows a more split-peak pattern for the mono-oxo structure, and spectrum (*B*) shows a merged-feature at 200~300 cm^{-1} with a small peak at ~370 cm^{-1} for the di-hydroxo structure.

1. Park K, et al. (2013) NRVS and DFT study of peroxo-bridged biferric complexes: Structural insight into peroxy intermediates of binuclear non-heme iron enzymes. *Angew Chem Int Ed* 52:1294–1298.

Table S1. Comparison with other vibrational spectroscopic data for 1

Fe(III)-μO-Fe(III) species	ν_s(Fe-μO)/cm$^{-1,a}$	ν_{as}(Fe-μO)/cm$^{-1,b}$	Fe-μO-Fe/°^{,c}
1	549 (−10)	714 (−34)	114
[Fe$_2$(μO)(tacn)$_2$(OAc)$_2$]$^{2+}$ (ref. 1)	540 (−17)	749 (−33)	119
[Fe$_2$(μO)(N3)$_2$(OBz)$_2$]$^{2+}$ (ref. 2)	537	745 (−45)	119
[Fe$_2$(μO)(HBpz$_3$)$_2$(OAc)$_2$] (ref. 3)	528 (−17)	749 (−30)	124

^{18}O isotopic shifts are given in parentheses. Each abbreviation indicates the following: tacn, 1,4,7-triazacyclononane; OAc, acetate; N3, bis(2-benzimidazolylmethyl)amine; OBz, benzoate; and HBpz$_3$, hydrotris(1-pyrazolyl)borate.
^{a}The frequencies of the symmetric Fe-μO stretch obtained from rR spectroscopy except for the NRVS data of **1**.
^{b}The frequencies of the antisymmetric Fe-μO stretch obtained from IR spectroscopy except for the NRVS data of **1**.
^{c}Fe-μO-Fe angle obtained from X-ray crystal structures. Ref. 2 showed that ν_s(Fe-μO) and ν_{as}(Fe-μO) are directly and inversely proportional to Fe-μO-Fe angle, respectively. Given this relation, the NRVS of **1** are consistent with the rR and IR data of related species.

1. Spool A, et al. (1985) Electronic and vibrational spectroscopic analysis of the (μ-oxo)bis(μ-carboxylato)diiron(III) core: a study of [Fe$_2$O(O$_2$CCH$_3$)$_2$(TACN)$_2$]$^{2+}$. *Inorg Chem* 24:2156–2162.
2. Sanders-Loehr J, et al. (1989) Electronic and Raman spectroscopic properties of oxo-bridged dinuclear iron centers in proteins and model compounds. *Inorg Chem* 111:8084–8093.
3. Armstrong W, et al. (1984) Assembly and characterization of an accurate model for the diiron center in Hemerythrin. *J Am Chem Soc* 106:3653–3667.

Table S2. Comparison with other vibrational spectroscopic data for 2

| Fe(III)-$(\mu O)_2$-Fe(IV) species | ν_s(Fe-μO)/cm^{-1} | |
	^{16}O	^{18}O
2	680	653
$[Fe_2(\mu O)_2(TPA)_2]$ $(ClO_4)_3$	666.1	633.9; 641.9 (637.9)
$[Fe_2(\mu O)_2(3\text{-}Me_3\text{-}TPA)_2]$ $(ClO_4)_3$	667	644; 628 (636)
$[Fe_2(\mu O)_2(5\text{-}Me_3\text{-}TPA)_2]$ $(ClO_4)_3$	676.7; 655.7 (666.2)	635

Values in parentheses indicate the center of a Fermi doublet. Except for the NRVS data of **2**, the frequencies of the Fe-μO stretch were obtained from rR data reported in ref. 1. Each abbreviation indicates the following: TPA, Tris(pyridyl-2-methyl)amine; 3-Me$_3$-TPA, Tris(3-methylpyridyl-2-methyl)amine; and 5-Me$_3$-TPA, Tris(5-methylpyridyl-2-methyl)amine.

1. Wilkinson EC, et al. (1998) Raman signature of the Fe$_2$O$_2$ "diamond" core. *J Am Chem Soc* 120:955–962.

Table S3. First-coordination sphere structures of X-ray crystal and DFT-optimized models of 1

| 1 | Xtal | BP/6–311G* | BP/6–31G* | B3LYP/6–31G* | 10% HF/90% BP + 6–31G* | | | |
	Fe^{3+}_2	Fe^{3+}_2	Fe^{3+}_2	Fe^{3+}_2	Fe^{3+}_2	$Fe^{3+}Fe^{4+}$	Fe^{4+}_2	hs **1**
Distance (Å)								
Fe1-O3	1.794	1.765	1.758	1.794	1.780	1.748	1.707	1.779
Fe1-O4	2.000	2.059	2.035	2.021	2.022	1.902	1.894	1.845
Fe1-N10	2.092	2.076	2.071	2.108	2.090	1.956	1.960	2.157
Fe1-N11	2.242	2.214	2.215	2.280	2.260	2.019	2.050	2.095
Fe1-N12	2.161	2.168	2.173	2.188	2.174	1.968	1.970	1.984
Fe1-N13	2.154	2.192	2.188	2.187	2.177	1.975	1.984	2.142
Fe2-O3	1.796	1.765	1.758	1.793	1.780	1.748	1.788	1.780
Fe2-O5	2.014	2.052	2.035	2.021	2.021	1.900	1.880	1.845
Fe2-N6	2.086	2.072	2.070	2.110	2.090	1.956	1.921	2.157
Fe2-N7	2.231	2.216	2.217	2.281	2.262	2.068	2.003	2.095
Fe2-N8	2.152	2.177	2.173	2.188	2.175	1.975	1.941	1.984
Fe2-N9	2.162	2.189	2.186	2.187	2.175	1.991	1.965	2.142
Fe1…Fe2	3.007	3.056	3.022	3.056	3.027	3.103	3.101	3.153
Angle (°)								
Fe1-O3-Fe2 (°)	113.7	120.0	118.5	116.8	116.5	125.2	125.0	124.7

Relevant structural formula and numbering scheme are shown in Fig. S5.

Table S4. First-coordination sphere structures of X-ray crystal and DFT-optimized models of 2

| 2 | Xtal (**2′**) | 10% HF/90% BP + 6–31G* | | |
	$Fe^{3+}Fe^{4+}$	$Fe^{3+}Fe^{4+}$	Fe^{4+}_2	hs **2**
Distance, Å				
Fe1-O3	1.805	1.814	1.880	1.784
Fe1-O4	1.860	1.740	1.743	1.823
Fe1-N5	2.050	2.022	1.991	2.096
Fe1-N6	2.003	2.012	1.995	1.968
Fe1-N7	2.026	1.972	1.975	2.193
Fe1-N8	2.025	1.971	1.975	2.193
Fe2-O3	1.860	1.806	1.743	1.823
Fe2-O4	1.805	1.865	1.880	1.784
Fe2-N9	2.003	1.979	1.995	1.968
Fe2-N10	2.050	1.985	1.991	2.096
Fe2-N11	2.025	1.969	1.975	2.193
Fe2-N12	2.026	1.968	1.975	2.193
Fe1…Fe2	2.683	2.647	2.726	2.673
Angle, °				
Fe1-O3-Fe2	94.1	94.0	97.5	95.6
Fe1-O4-Fe2	94.1	94.4	97.5	95.6
O3-Fe1-O4	85.9	87.5	82.5	84.4
O3-Fe2-O4	85.9	84.1	82.5	84.4

Relevant structural formula and numbering scheme are shown in Fig. S5.

Table S5. Force constants obtained from NCA for low and high spin 1

Force constants	Internal coordinate	ls 1	hs 1
Bonds, mdyne/Å	Fe1-O3	2.6	2.0
	Fe1-O4	1.5	1.0
	Fe1-N10	0.85	0.40
	Fe1-N11	1.5	0.75
	Fe1-N12	1.5	0.75
	Fe1-N13	0.85	0.40
	O4-C14	6.0	6.0
	C14-N6	6.0	6.0
	Fe2-O3	2.6	2.0
	Fe2-O5	1.5	1.0
	Fe2-N6	0.85	0.40
	Fe2-N7	1.5	0.75
	Fe2-N8	1.5	0.75
	Fe2-N9	0.85	0.40
	O5-C15	6.0	6.0
	C15-N10	6.0	6.0
Angles, mdyne·Å	Fe1-O3-Fe2	0.35	0.60
	O3-Fe1-O4	0.35	0.65
	O3-Fe1-N10	0.75	0.40
	O3-Fe1-N12	0.75	0.65
	O3-Fe1-N13	0.75	0.40
	N11-Fe1-O4	0.75	0.65
	N11-Fe1-N10	0.35	0.33
	N11-Fe1-N12	0.65	0.65
	N11-Fe1-N13	0.35	0.33
	O4-Fe1-N10	0.75	0.40
	O4-Fe1-N13	0.75	0.40
	N10-Fe1-N12	0.35	0.35
	N12-Fe1-N13	0.35	0.35
	Fe1-O4-C14	0.40	0.35
	Fe1-N10-C15	0.40	0.35
	O4-C14-N6	1.4	1.2
	O3-Fe2-O5	0.35	0.65
	O3-Fe2-N6	0.75	0.40
	O3-Fe2-N8	0.75	0.65
	O3-Fe2-N9	0.75	0.40
	N7-Fe2-O5	0.75	0.65
	N7-Fe2-N6	0.35	0.35
	N7-Fe2-N8	0.65	0.65
	N7-Fe2-N9	0.35	0.35
	O5-Fe2-N6	0.75	0.40
	O5-Fe2-N9	0.75	0.40
	N6-Fe2-N8	0.35	0.33
	N8-Fe2-N9	0.35	0.33
	Fe2-O5-C15	0.40	0.35
	Fe2-N6-C14	0.40	0.35
	O5-C15-N10	1.4	1.2
Interactions	Fe1-O3/Fe1-O3-Fe2	0.05	−0.2
	Fe2-O3/Fe1-O3-Fe2	0.05	−0.2
	Fe1-O3/O3-Fe1-O4	0.10	0
	Fe2-O3/O3-Fe2-O5	0.10	0
	Fe1-O3/O3-Fe1-N12	0.20	0
	Fe2-O3/O3-Fe2-N8	0.20	0

Table S6. Force constants obtained from NCA for low and high spin 2

Force constants	Internal coordinate	ls 2	hs 2
Bonds, mdyne/Å	Fe1-O3	1.7	2.4
	Fe1-O4	1.9	1.5
	Fe1-N5	1.2	0.85
	Fe1-N6	1.8	0.95
	Fe1-N7	0.85	0.45
	Fe1-N8	0.85	0.45
	Fe2-O3	1.5	2.0
	Fe2-O4	2.4	1.0
	Fe2-N9	1.8	0.95
	Fe2-N10	1.2	0.85
	Fe2-N11	0.95	0.45
	Fe2-N12	0.85	0.45
Angles, mdyne·Å	Fe1-O3-Fe2	0.35	0.95
	O3-Fe1-O4	0.50	0.85
	O3-Fe1-N6	0.75	0.60
	O4-Fe1-N5	0.75	0.60
	N5-Fe1-N6	0.65	0.40
	O3-Fe1-N7	0.80	0.40
	O3-Fe1-N8	0.80	0.40
	O4-Fe1-N7	0.80	0.40
	O4-Fe1-N8	0.80	0.40
	N5-Fe1-N7	0.40	0.33
	N5-Fe1-N8	0.40	0.33
	N6-Fe1-N7	0.45	0.35
	N6-Fe1-N8	0.45	0.35
	Fe1-O4-Fe2	0.35	0.95
	O3-Fe2-O4	0.50	0.85
	O3-Fe2-N10	0.75	0.60
	O4-Fe2-N9	0.75	0.60
	N9-Fe2-N10	0.65	0.40
	O3-Fe2-N11	0.80	0.40
	O3-Fe2-N12	0.80	0.40
	O4-Fe2-N11	0.80	0.40
	O4-Fe2-N12	0.80	0.40
	N9-Fe2-N11	0.45	0.35
	N9-Fe2-N12	0.45	0.35
	N10-Fe2-N11	0.40	0.33
	N10-Fe2-N12	0.40	0.33
Interactions	Fe1-O3/Fe1-O3-Fe2	−0.2	0.1
	Fe2-O4/Fe1-O4-Fe2	−0.2	0.1
	Fe1-O3/O4-Fe1-N5	0.50	0.30
	Fe1-O4/O3-Fe1-N6	0.50	0.70
	Fe1-N6/O3-Fe1-N6	0.50	0.10
	O3-Fe1-N7/N5-Fe1-N8	0.05	−0.05
	O3-Fe1-N8/N5-Fe1-N7	0.05	−0.05
	O4-Fe1-N7/N6-Fe1-N8	0.05	−0.05
	O4-Fe1-N8/N6-Fe1-N7	0.05	−0.05
	O3-Fe1-O4/N5-Fe1-N6	0	0.30
	Fe1-O4/Fe1-O4-Fe2	0.2	0.1
	Fe2-O3/Fe1-O3-Fe2	0.2	0.1
	Fe2-O4/O3-Fe2-N10	0.50	0.30
	Fe2-O3/O4-Fe2-N9	0.50	0.70
	Fe2-N9/O4-Fe2-N9	0.50	0.10
	O4-Fe2-N11/N10-Fe2-N12	0.05	−0.05
	O4-Fe2-N12/N10-Fe2-N11	0.05	−0.05
	O3-Fe2-N11/N9-Fe2-N12	0.05	−0.05
	O3-Fe2-N12/N9-Fe2-N11	0.05	−0.05
	O3-Fe2-O4/N9-Fe2-N10	0	0.30